Int. J. Solids Structures Vol. 22, No. 7, pp. 693–708, 1986
Printed in Great Britain.

0020-7683/86 $3.00 + .00
Pergamon Journals Ltd.

ON J-DOMINANCE OF CRACK-TIP FIELDS IN LARGELY YIELDED 3D STRUCTURES

WOLFGANG BROCKS
Bundesanstalt für Materialprüfung, Berlin, Federal Republic of Germany

and

JÜRGEN OLSCHEWSKI
Hahn-Meitner-Institut für Kernforschung, Berlin, Federal Republic of Germany

(*Received* 28 *June* 1985)

Abstract—The *J*-integral has been widely accepted as a parameter characterizing the load intensity in nonlinear fracture mechanics. Nevertheless, a theoretical foundation of the *J* concept for a three-dimensional flawed structure in large-scale yielding assuming incremental theory of plasticity is still missing. Only numerical studies may help to close this gap. The questions to be answered are, how a significant value of *J* can be defined, by which method it can be calculated, and to what extent it will dominate the stress and strain field in the vicinity of a crack. Finite element calculations using von Mises flow theory and large strain formulation have been accomplished on different kinds of structures with both straight and semi-elliptical cracks. The results showed that the *J*-integral may be defined locally in a largely yielded three-dimensional structure by the energy release rate due to "virtual" crack extension and that this quantity seems to dominate the local stress and strain field in some confined area ahead of the crack front. As this relationship appeared to be a power law of J/r the FE results have been compared with the plane strain HRR solutions. Though the results agreed satisfactory well, some phenomena of the plastic response of the material could not be explained by the HRR theory. Especially, the problem how to find appropriate values for the parameters α and n of the Ramberg–Osgood hardening law for any real material has remained an open question.

INTRODUCTION

Any engineer being concerned about structural integrity of components will need some mechanical parameter which has to be a geometric invariant quantity, so that the critical value for "failure" can be determined from a laboratory specimen and used in a wide variety of engineering structures of different load configurations, shapes, and sizes. For high-strength, relatively brittle materials as well as for fatigue crack growth and corrosion cracking the linear elastic fracture mechanics and its concept of stress intensity factor have found extensive application supposing that the plastic zone is small enough. However, many components are made of ductile materials and will, under practical operating conditions, become fully plastic before a crack starts to advance under monotonic loading. It is therefore essential to consider the plastic behaviour of structures.

Nonlinear fracture mechanics based on the assumption of "*J*-control" is a semi-empirical approach which is widely accepted for failure assessment in large-scale yielding[1]. The analytical background of this approach is the idea of a path independent contour integral around the crack tip[2] which characterizes the load intensity and, hence, dominates the singular crack-tip field. Assuming a power law hardening this dominance is described analytically by the HRR equations[3, 4]. Nevertheless, the theoretical background of the *J*-integral approach is not a very solid one because the material model behind it is a small strain deformation theory of plasticity which, in general, does not meet the crack tip situation in a real ductile material.

Proving the path independence of the *J*-integral means proving a conservation law and, hence, postulating a nonlinearly elastic behaviour which is the essential of deformation theory. Thus, not only local unloading, which will occur when the crack propagates, has to be disregarded but also proportional loading must be assumed, that means a constant ratio of principal stresses during the load history. Any rearrangement of stresses in the process zone of the blunting crack tip will violate this basic assumption of the model. Consequently, McMeeking[5] found that the *J*-integral has significant path dependence

immediately adjacent to a blunted crack tip. Obviously, the value of the contour integral even tends to zero as the integration path shrinks to the crack tip because the singularity of the stress field has vanished with increasing plastic strain.

A second lack of the model is that the original J-integral as introduced by Rice as well as the HRR equations represent a plane situation, only, whereas in a real structure there is a stress and strain gradient along the crack front and, in addition, the crack front may be curved. An extension of J to three dimensions can be given by introducing a plane subregion of infinitesimal constant thickness perpendicular to the crack front in any point. The value of the contour integral in this subregion is referred to as the "local" J-value[6]. But a corresponding analytical solution of the three-dimensional boundary value problem at the crack tip which might reveal the significance of the so defined local J as an intensity parameter for the local stress and strain field is still missing and will probably never be possible.

Thus, only numerical methods are available to study the significance of J in three dimensions at large plastic strain and incremental plasticity. Several authors have investigated large-scale yielding of cracked bodies and the influence of finite deformations at the crack tip to find criteria for J-dominance[7–10]. But these investigations are all restricted to plane strain conditions and, mostly, to deformation theory. In the present study, comparative three-dimensional elastic plastic finite element (FE) calculations have been accomplished using the incremental Prandtl–Reusz flow theory in an updated Lagrangian formulation allowing for large strain.

INVESTIGATED STRUCTURES AND FE MODELS

Five different sizes of compact tension (CT) specimens have been analyzed[11] which are, with the exception of one, standard test specimens according to ASTM E 399 with a crack length to width ratio of $a/W = 0.5$ (Fig. 1). Their thickness $B = W/2$ varied from 12.5 mm (CT 12.5) to 200 mm (CT 200). The nonstandard specimen was only half as thick as required to study the influence of specimen thickness and is referred to as "CT 200 (B/2)". The FE mesh in the vicinity of the crack tip was taken the same for all sizes. The

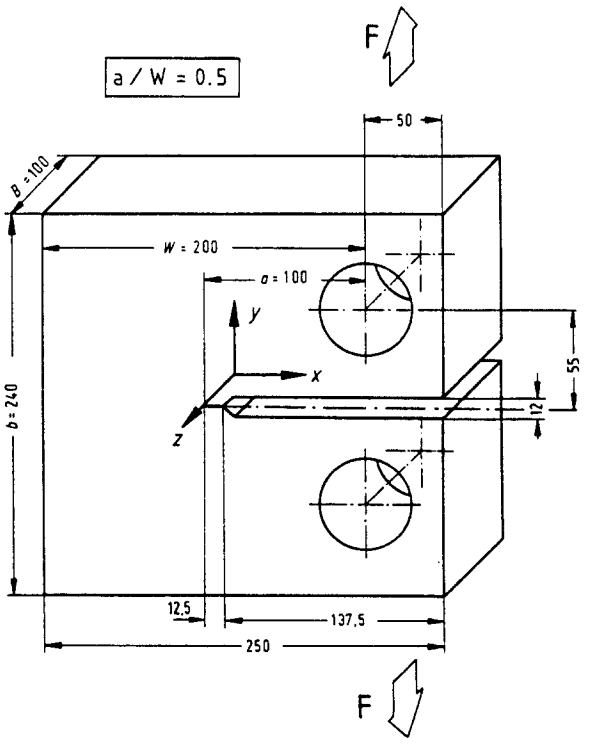

Fig. 1. Compact tension (CT) specimen, dimensions of the standard CT 100 (ASTM E 399).

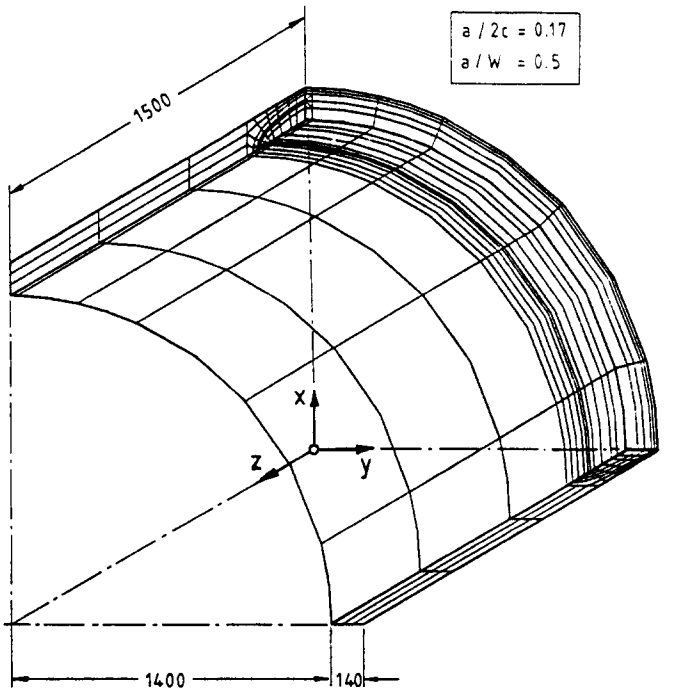

Fig. 2. Pressurized cylinder, dimensions and FE mesh of 1/8 sector of the structure.

CT specimen represents a rather simple plane configuration because all cross sections z = const are congruent, the crack front is straight, and the external forces act uniaxial and inplane. Besides, it plays the role of a reference state of stress because, usually, critical J-values for initiation of crack growth are obtained from it.

The second structure was a pressurized cylinder with a semi-elliptical inner surface flaw in axial direction (Fig. 2). Its inner radius is $R_i = 1400$ mm and its wall thickness $W = 0.1R_i$. It is not subjected to axial forces, and any pressure on the crack surface is neglected as well. The depth to length ratio of the crack is $a/2c = 0.17$ and it penetrates to 59% of the wall thickness. Though the crack front is not straight any more the remote stress state is still a very simple one because it is mainly tension by an approximately constant hoop stress. However, the problem of a flawed pressure vessel is of great practical relevance[12].

The third structure has been developed as a specimen to study the influence of multiaxial loading[13]. It is a thick plate of dimensions 1000 × 140 mm under 8-point bending bearing a semi-elliptical surface crack (Fig. 3). Thus, it is subjected to biaxial bending in the x- and z-axis. The crack shape is the same as for the cylinder (Fig. 4).

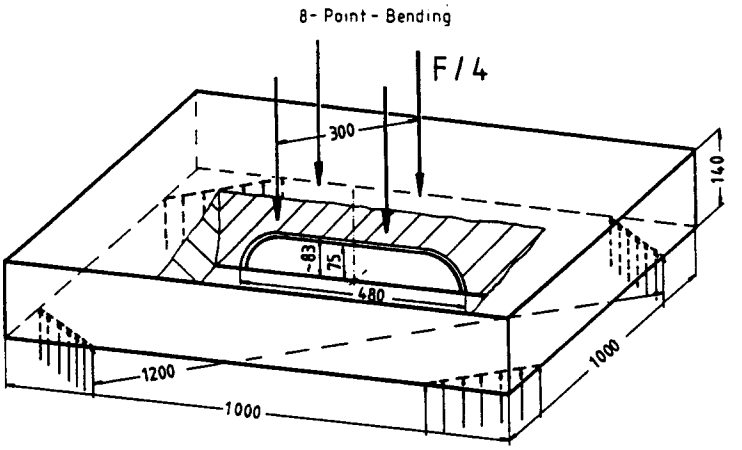

Fig. 3. Plate under 8-point bending, dimensions and load configuration of the structure.

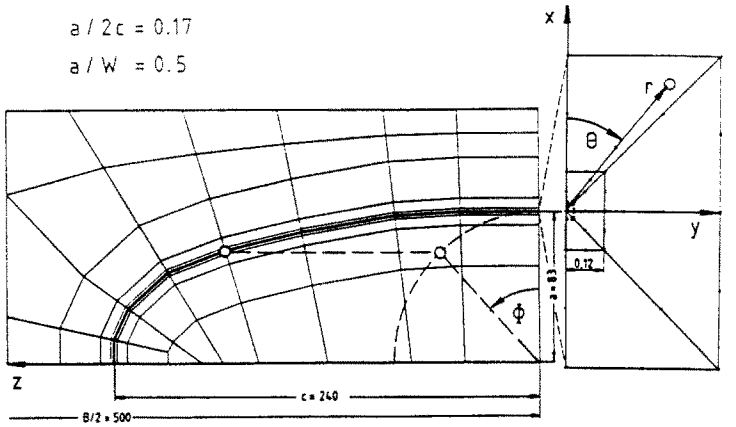

Fig. 4. Semi-elliptical surface crack, coordinate system and FE mesh of the crack plane.

The material was chosen to be the same for all structures. Its yield strength of $\sigma_0 = 440$ MPa and the uniaxial yield curve have been obtained from test specimens of the German reactor steel 20 Mn Mo Ni 5 5 which is similar to the American steel A 533 B used for the same kind of applications. The yield curve has been approximated by a multilinear curve (Fig. 5). Thus, no *a priori* approximation of the material hardening by a Ramberg–Osgood power law has been introduced into the FE analysis. The dashed curve in Fig. 5 represents only the reference values used for comparing the FE results with the HRR solutions, which will be discussed later.

The computer code ADINA[14] was used for the FE calculations being extended by some capabilities to calculate the J-integral[15]. Because of a number of numerical difficulties, the calculation of J in a three-dimensional cracked body is not commonly based on the contour integral definition but on the idea of released energy by a "virtual" crack extension, which has originally been developed by Parks[16] and carried out for elastic plastic material by de Lorenzi[17]. A detailed description together with numerical results of both methods, contour integral and virtual crack extension, may be found in Ref. [6]. The background of the latter algorithm is a merely mathematical one of converting a contour to a domain integral and must not be mistaken for a physical process, since a "real" extension of a crack in an elastic plastic body will result in local unloading. A physical equivalence does only exist for an elastic material. Hence, this method which is also used

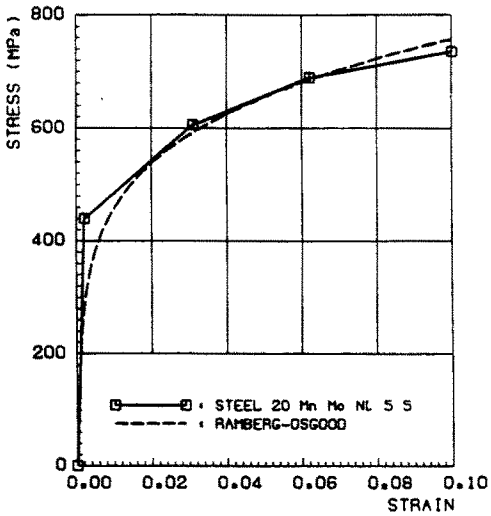

Fig. 5. Uniaxial true stress true strain curve of steel 20 MnMoNi 5 5; Ramberg–Osgood approximation ($\alpha = 3.07$, $n = 5.00$).

in the present study may be understood either as a "virtual" or "fictitious" crack extension in a real elastic plastic material or as a real crack propagation in a fictitious nonlinear elastic material.

RESULTS

If the J-integral is supposed to be a unifying parameter to characterize the local load intensity at arbitrarily shaped cracks in a large variety of structures under different load conditions it must at least be possible to specify its value uniquely. As mentioned before, it will become "path dependent" as soon as plastic flow occurs. However, since the contour integral definition is not used here the concept of a "path" is senseless, anyhow, and talking of "path dependence" may be misleading. A new definition of this idea has to be given. In order to calculate the energy release rate by virtual crack extension some subdomain at the crack front has to be shifted by a small amount. As any subdomain in the model is represented by finite elements this means shifting of rings of nodes around the crack tip. By varying the number of node rings to be shifted one will, in general, obtain different results for J which will be referred to as "path dependence". Two typical examples are given in Figs. 6(a) and (b) showing the results for the pressurized cylinder at two points of the crack front which are characterized by the angle ϕ as defined in Fig. 4. Obviously, the path dependence increases with increasing pressure, that is with extension of the plastic zones. But if a sufficient number of node rings has been shifted the value obtained becomes stationary. The so defined stationary or remote value will be taken for J.

The following figures show the variation of the local J along the crack front under increasing load for the CT 100 (Fig. 7), the pressurized cylinder (Fig. 8), and the bending plate (Fig. 9). The differences between the three different geometries and load configurations are reflected clearly by the J-curves. In the CT specimen, J has a maximum in the mid-plane which coincides with the maximum of stresses and crack tip opening and which does not alter its position when load increases. The situation is only slightly different for the semi-elliptical surface crack in the cylinder. For low pressure, when the structure is nearly fully elastic, the J-distribution starts with three local maxima, two at the penetration points of the crack front with the inner surface and one at the deepest point of the crack. It ends, for high pressure, with just one maximum in the centre. The remote stress field is similar for the cylinder and for the CT specimen and therefore the J-distributions of both structures could be expected to be qualitatively similar. This is completely different in the bending plate, where J has two maxima near the free surface which shift to the region of strong

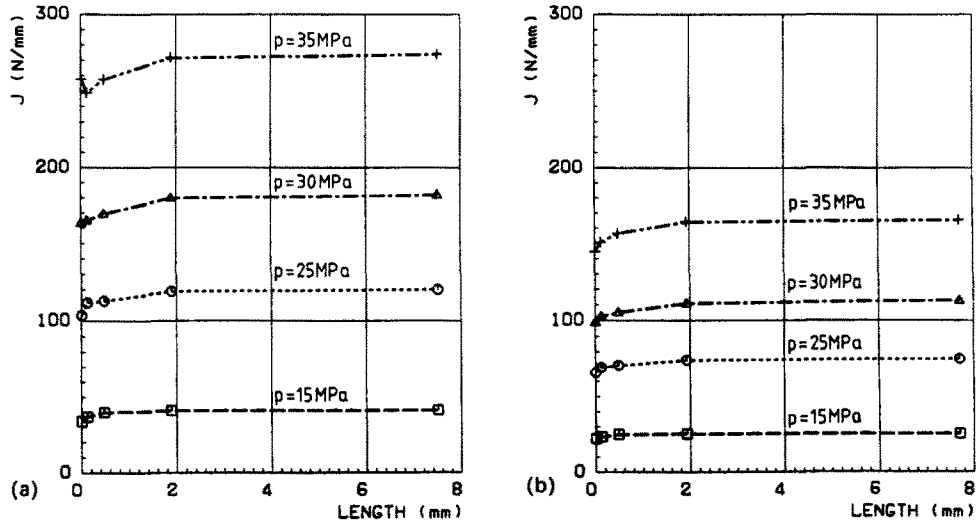

Fig. 6. (a) J-Integral vs extension of shifted subdomain showing "path dependence" for the pressurized cylinder at $\phi = 0$ deg. (b) J-Integral vs extension of shifted subdomain showing "path dependence" for the pressurized cylinder at $\phi = 81$ deg.

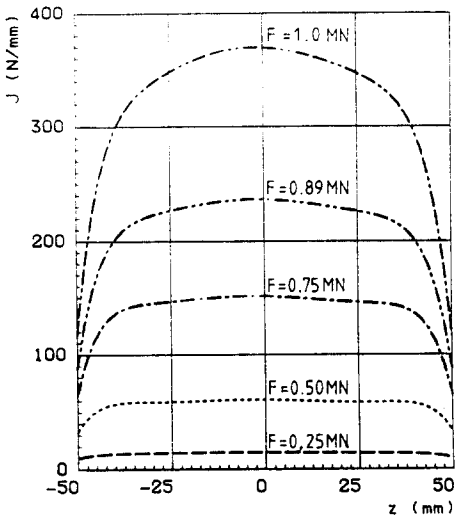

Fig. 7. J-Integral along the crack front of the CT 100 specimen for increasing load F.

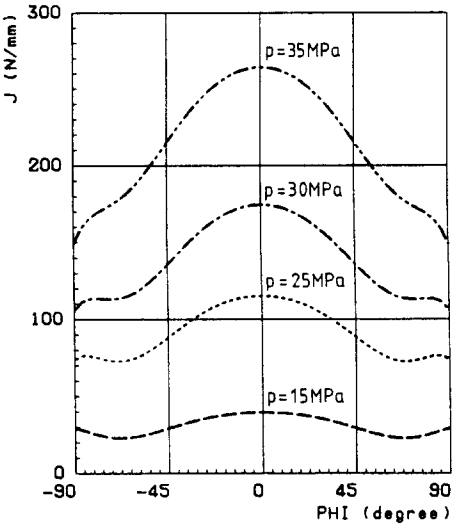

Fig. 8. J-Integral along the crack front of the cylinder under increasing pressure p.

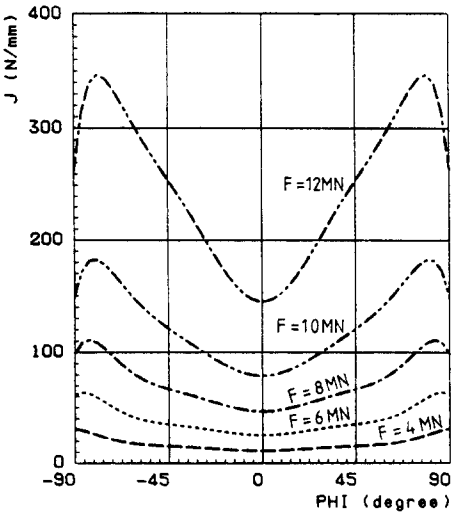

Fig. 9. J-Integral along the crack front of the plate under 8-point bending for increasing load F.

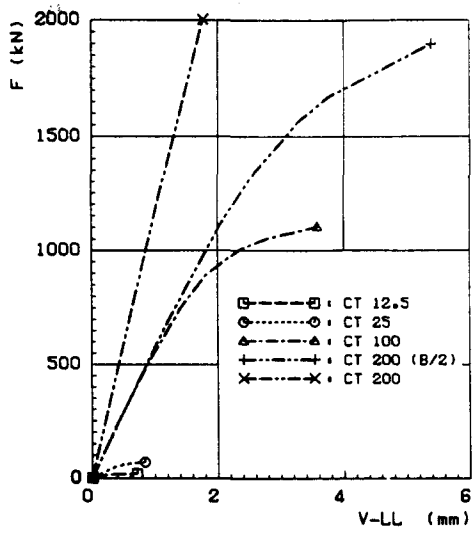

Fig. 10. Load F vs load line displacement V_{LL} for various sizes of compact tension specimens.

curvature of the ellipse when load increases but remain far away from the deepest point of the crack. The differences in the J-distribution of plate and cylinder are due to the different nominal stress states which are bending and tension, respectively.

Next, the effect of specimen size shall be looked at. The large differences in nonlinear behaviour of the five CT specimens are illustrated by the load vs load line displacement plot in Fig. 10 and by the extension of the plastic zones at a given J in Fig. 11. All situations from small to large scale yielding are represented, and J is expected to characterize the whole bandwidth of nonlinearities. The five load vs displacement curves can easily be approximated by one "master curve" if the load F is normalized by the plastic limit load F_0 and the load line displacement V_{LL} by the crack length (Fig. 12), remembering that a/W is a constant. The plastic limit loads of the standard specimens which were found from the FE calculations coincided with less than 1% error with the formula given by Shih *et al.*[10]. As the load vs displacement curves can be fitted by one master curve the same can be done with the J-integral vs the applied load (Fig. 13) if the quantities are normalized appropriately.

In further evaluations of stresses and strains J turned out to be a significant parameter which dominates the crack tip fields independently of specimen size. Figure 14 gives just one example showing the crack opening stresses σ_{yy} in the ligament of the mid-plane at approximately $J = 140$ N/mm for the various specimen sizes. This is by no means obvious because the extent of plastification is quite different, as Fig. 11 has shown, and a geometrically nonlinear, incremental theory has been used for the calculations. Since J dominates the strain field around the crack tip one should expect a unique relationship between J and

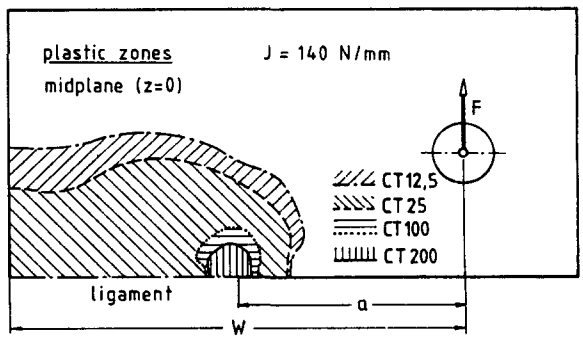

Fig. 11. Compact tension specimens, plastic zone size at similar J-values for various specimen sizes.

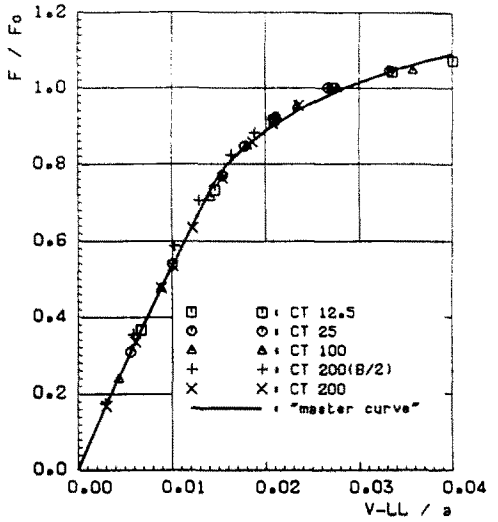

Fig. 12. Load F vs load line displacement V_{LL}, normalized by plastic limit load F_0 and crack length a for various CT specimen sizes.

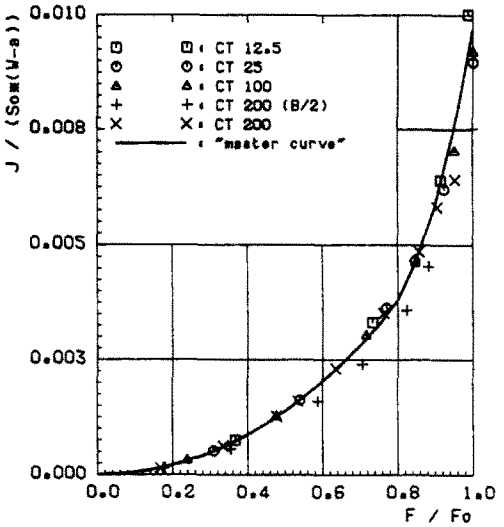

Fig. 13. J-Integral vs load F normalized by yield strength S_0, ligament size W/a and plastic limit load F_0 for various CT specimen sizes.

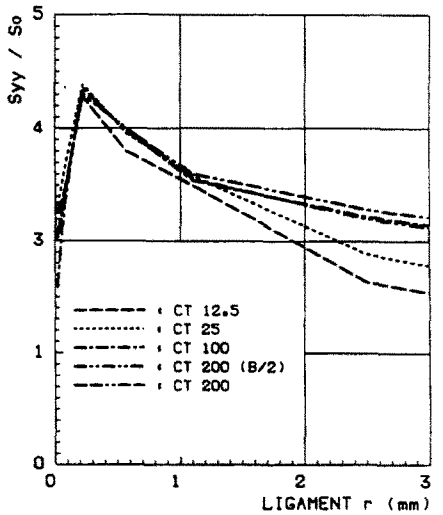

Fig. 14. Crack opening stresses in the ligament, normalized by yield strength S_0 for various CT specimen sizes at approximately $J = 140$ N/mm.

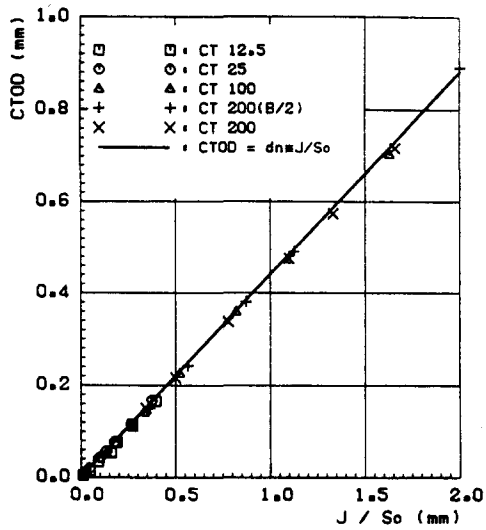

Fig. 15. Crack tip opening displacement in the midplane vs J-integral normalized by yield strength S_0 for various CT specimen sizes.

the crack tip opening displacement (CTOD) as well. Figure 15 confirms the linear relation

$$\delta_t = d_n J/\sigma_0, \tag{1}$$

where d_n is a constant depending on the material and, in a 2D model, on the geometric condition of plane stress or plane strain[10]. Thus, if J is an appropriate parameter to describe fracture phenomena, CTOD is one as well. However, it is much easier to calculate δ_t in an FE model than to measure it on a test specimen.

After all, no significant size dependencies were found with respect to stress and strain fields if J (or CTOD) were taken as quantities characterizing the load intensity. Hence, the results of the CT 100 may be taken as reference values in the further discussions which will now be concerned with the comparison of different load and geometry configurations as represented by the CT specimen, the pressurized cylinder, and the plate under 8-point bending. Despite all obvious differences between these different structures the local J-value turned out to be a dominating quantity for stress and strain fields again. First, the same linear relationship of eqn (1) was found throughout the crack front between the local J and the local δ_t for the pressurized cylinder (Fig. 16) as well as for the bending plate (Fig. 17), with the exception of points where the crack penetrates the free surface ($\phi = 90°$).

Since CTOD appeared to be a quantity characterizing the local load intensity, the different stress curves of varying load and/or varying ϕ, except for $\phi = 90°$, will collapse to one curve if the distance r from the crack tip is normalized by the local δ_t. In addition, plots of σ_{yy} vs r/δ_t on a log–log scale (Figs. 18–20) reveal a region of a power law dependency between both quantities

$$\ln(\sigma_{yy}/\sigma_0) = \ln C - m \ln(r/\delta_t) \tag{2}$$

or

$$\frac{\sigma_{yy}}{\sigma_0} = C\left(\frac{\delta_t}{r}\right)^m. \tag{3}$$

This region is bounded by approximately

$$2\delta_t \leqslant r \leqslant 50\delta_t. \tag{4}$$

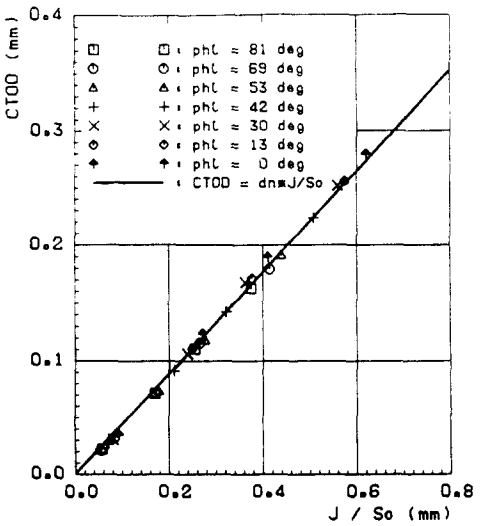

Fig. 16. Local crack tip opening displacement vs J-integral normalized by yield strength S_0 along the crack front in the pressurized cylinder.

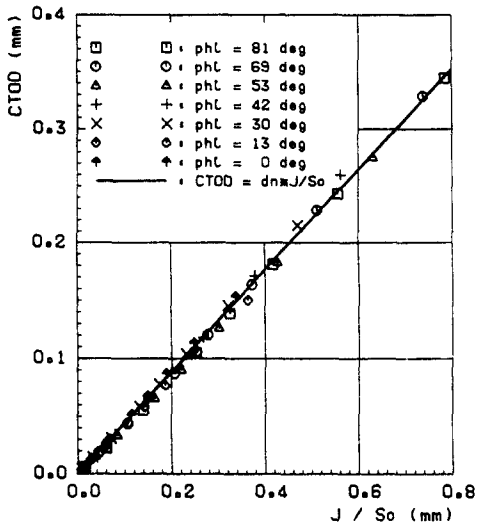

Fig. 17. Local crack tip opening displacement vs J-integral normalized by yield strength S_0 along the crack front in the plate under 8-point bending.

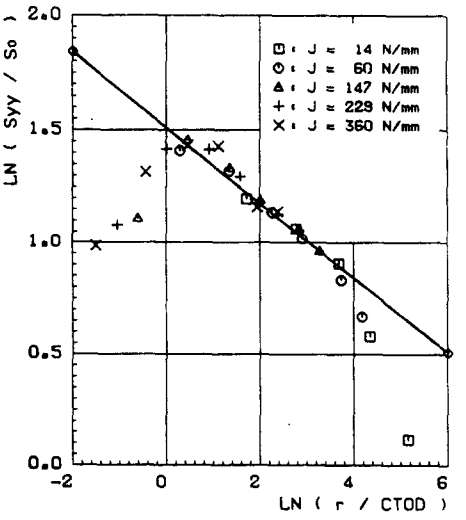

Fig. 18. Crack opening stresses in the ligament of the CT 100 specimen normalized by yield strength S_0 and crack tip opening displacement (CTOD), determination of the Ramberg–Osgood parameters $\alpha = 3.07$, $n = 5.00$.

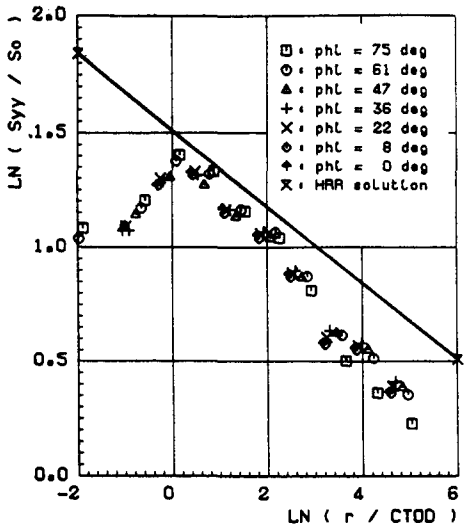

Fig. 19. Crack opening stresses in the ligament of the pressurized cylinder at $p = 35$ MPa normalized by yield strength S_0 and crack tip opening displacement (CTOD).

The slope m in eqn (2) does not differ very much between the different structures and, hence, may be regarded as a material constant which is independent of the geometry. In the present study, its value is approximately $m = 1/6$. Though in Figs. 19 and 20 only the stresses σ_{yy} in the ligament are plotted for just one load step, the relation holds for all load steps, and similar correlations will be found for the other stress components as well. This encourages the idea of comparing the FE results with the HRR plane strain solutions.

Comparison with the HRR field

Introducing the linear relationship between J and CTOD, the HRR equations for the singular stress and strain field at the crack tip take the form

$$\left.\begin{aligned}\sigma_{ij}(r,\theta) &= \sigma_0\left(\frac{E}{\alpha\sigma_0 I_n d_n}\right)^{\frac{1}{n+1}}\left(\frac{\delta_t}{r}\right)^{\frac{1}{n+1}}\tilde{\sigma}_{ij}(\theta)\\ \varepsilon_{ij}(r,\theta) &= \alpha\varepsilon_0\left(\frac{E}{\alpha\sigma_0 I_n d_n}\right)^{\frac{n}{n+1}}\left(\frac{\delta_t}{r}\right)^{\frac{n}{n+1}}\tilde{\varepsilon}_{ij}(\theta)\end{aligned}\right\}, \tag{5}$$

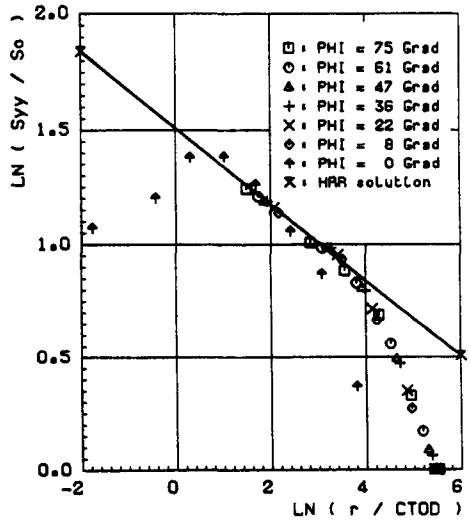

Fig. 20. Crack opening stresses in the ligament of the plate under 8-point bending at $F = 12$ MN normalized by yield strength S_0 and crack tip opening displacement (CTOD).

where α, n, σ_0, ε_0 are the constitutive coefficients of the Ramberg–Osgood power law, E is Young's modulus, d_n is the factor in eqn (1), I_n is an integration constant depending on n, and $\tilde{\sigma}_{ij}$, $\tilde{\varepsilon}_{ij}$ are dimensionless functions of the ligament angle θ (see Fig. 4).

The first step is to find appropriate values for the coefficients of the hardening law which, in general is a difficult task because no real material fits a power curve over a large range of deformation. Usually σ_0 is taken as the yield strength and $\varepsilon_0 = \sigma_0/E$. Hence, α and n are left as free parameters. Here, these parameters were not evaluated by fitting the material hardening curve (Fig. 5) but by approximating the FE stresses σ_{yy} in the ligament of the CT 100 (Fig. 18), *a posteriori*. It follows from eqns (3) and (5) that

$$m = 1/(n+1)$$
$$C = (\alpha\sigma_0 I_n/E)^m \tilde{\sigma}_{yy}(\theta = 0) \tag{6}$$

and taking $m = 1/6$ as in Fig. 18 we get $n = 5.0$ and $\alpha = 3.07$ if the plane strain solution is taken as reference. The corresponding hardening curve is given by the dashed line in Fig. 5. It is now possible to compare all stress components at any angle θ to the ligament which have been obtained by a 3D large strain elastic–plastic FE analysis with the 2D small strain deformation theory solution. Only a few examples can be given here showing good agreements in some cases and disagreements in some others. The examples are restricted to the CT specimens as some discussion might arise how the x- and z-direction should be defined for the curved crack front.

First, the variation of stresses with the distance coordinate r under a fixed angle θ is plotted for a given load intensity of $J = 140$ N/mm which is beyond the plastic limit load for the two smaller specimens (see Fig. 11). If we look at the smallest principal stress σ_{xx} in the ligament, we will find a rather good approximation beyond the locus of the stress maximum which lies at about $5\delta_t$ ahead of the crack tip (Fig. 21). At the crack tip ($r = 0$), of course, HRR stresses become singular whereas for a large strain solution σ_{xx} has to be zero because of the boundary condition. This discrepancy does not arise for the shear stress σ_{xy} at $\theta = 90°$ as Fig. 22 shows. Since the FE stresses result from a 3D solution the hydrostatic (or mean) stress σ_m is expected to be overestimated by the HRR equations which assume plane strain condition (Fig. 23). However, the approximation of the von Mises effective stress $\bar{\sigma}$ in the ligament turned out to be very bad. The HRR values lie more than 50% lower than the FE results, but this effect will be discussed later. For ductile fracture phenomena, the "triaxiality" is defined as the ratio of hydrostatic to effective stress.

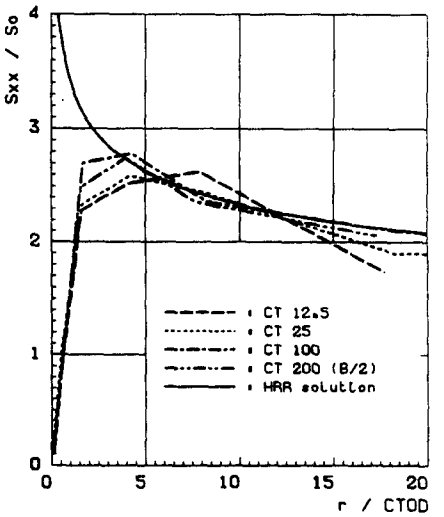

Fig. 21. Normal stresses σ_{xx} in the ligament normalized by yield strength S_0 and crack tip opening displacement for various CT specimen sizes at approximately $J = 140$ N/mm.

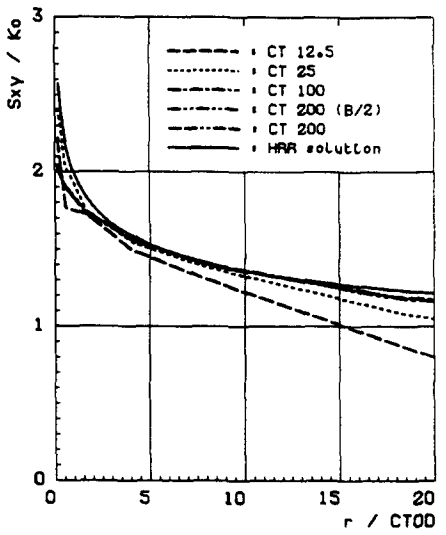

Fig. 22. Shear stress at 90 deg. to the ligament normalized by $K_0 = S_0/\sqrt{3}$ and crack tip opening displacement for various CT specimen sizes at approximately $J = 140$ N/mm.

HRR theory predicts that this quantity does neither depend on the distance coordinate r nor on the load intensity because according to eqn (5) any quotient of two stress components is a constant with respect to both quantities. This was found not to be true in the FE analysis.

A few examples will be given, finally, for the variation of stresses with the ligament angle θ at a constant distance of $r = 0.23$ mm. The stress components σ_{xx} (Fig. 24), σ_{yy} (Fig. 25), and the hydrostatic stress σ_m (Fig. 26) show the same qualitative distributions comparing FE and HRR solutions whereas the quantitative deviations differ. All together, the agreement has to be called satisfactory considering how many of the basic assumptions of HRR theory have been violated. The best coincidence, of course, is found for σ_{yy} at $\theta = 0$ where the curve fitting for the Ramberg–Osgood coefficients α and n took place. However, major differences occur for the shear stresses σ_{xy} (Fig. 27) and consequently for the effective stress $\bar{\sigma}$ (Fig. 28) at $\theta \leqslant 45°$. Shear stresses do not even have the same sign, and at 45° HRR theory predicts them to vanish while the FE values equal the yield stress in shear $K_0 = \sigma_0/\sqrt{3}$. This results in an underestimate of effective stress in that region which has been stated above, already.

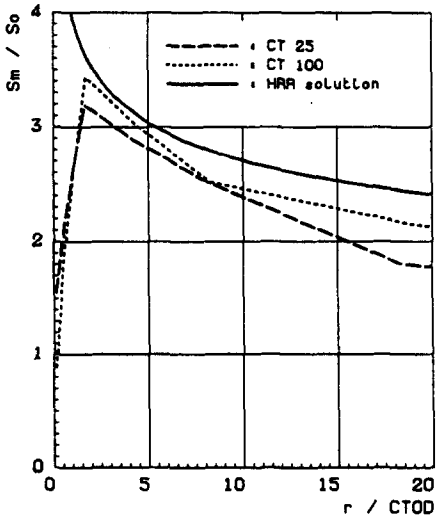

Fig. 23. Mean (hydrostatic) stress in the ligament normalized by yield strength S_0 and crack tip opening displacement (CTOD) for two CT specimen sizes at approximately $J = 140$ N/mm.

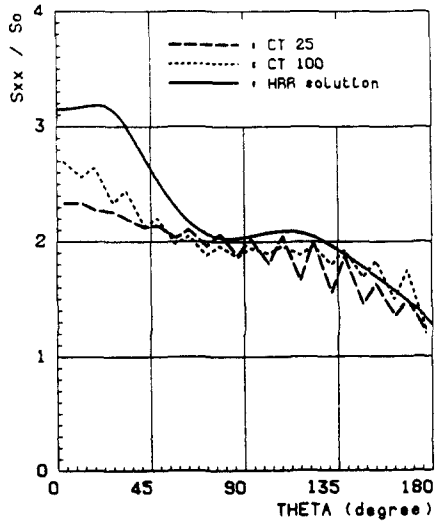

Fig. 24. Normal stresses σ_{xx} around the crack tip in a distance of $r = 0.23$ mm normalized by yield strength S_0 for two CT specimen sizes at approximately $J = 140$ N/mm.

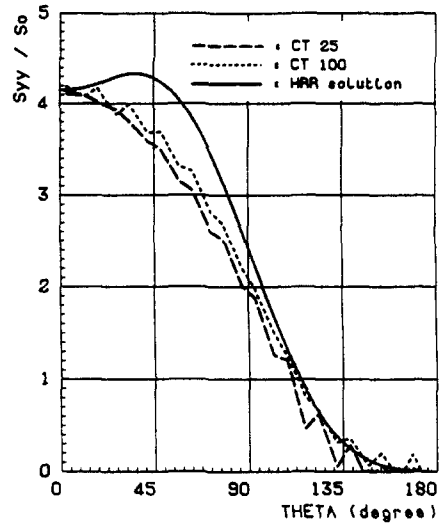

Fig. 25. Crack opening stresses around the crack tip in a distance of $r = 0.23$ mm normalized by yield strength S_0 for two CT specimen sizes at approximately $J = 140$ N/mm.

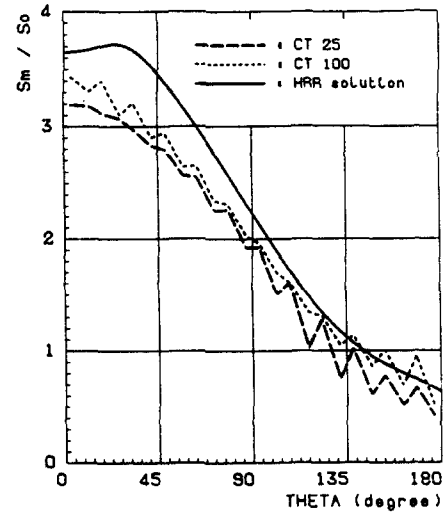

Fig. 26. Mean stresses around the crack tip in a distance of $r = 0.23$ mm normalized by yield strength S_0 for two CT specimen sizes at approximately $J = 140$ N/mm.

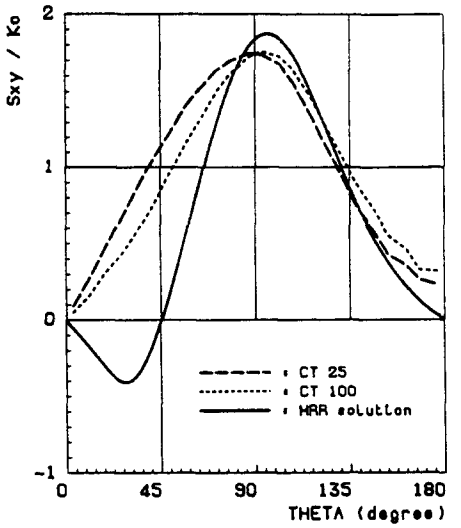

Fig. 27. Shear stresses around the crack tip in a distance of $r = 0.23$ mm normalized by $K_0 = S_0/\sqrt{3}$ for two CT specimen sizes at approximately $J = 140$ N/mm.

CONCLUSIONS

(1) Only experiments can measure a material's resistance to fracture. But analytical and numerical investigations are the necessary means to define characteristic quantities which may be supposed as being independent of the structure geometry and, hence, being material parameters.

(2) A local value of the J-integral can be defined and calculated in a 3D structure along an arbitrarily shaped crack even for large plastic strain. Though it is not path independent in a strict sense it takes a stationary value somewhat remote from the crack tip. This remote value is a measure of the local load intensity and dominates the local stress and strain field in a confined region ahead of the crack tip, independently of the geometry and load configuration of a flawed structure.

(3) A linear relation exists between the local J and the local crack tip opening displacement CTOD which depends on the material properties, mainly. Thus, if J is a characteristic parameter for crack initiation, CTOD is one as well.

(4) In some region ahead of the crack tip the stresses and strains in a 3D body can be

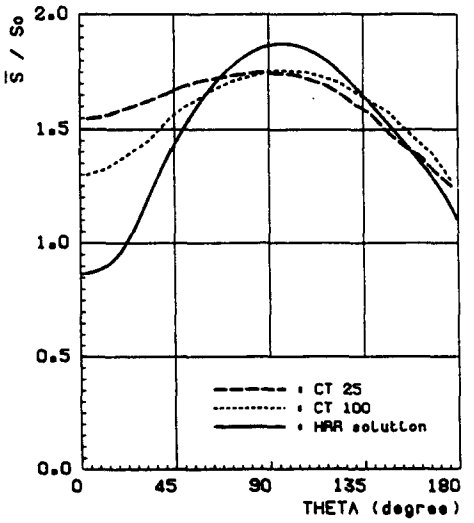

Fig. 28. Equivalent stresses around the crack tip in a distance of $r = 0.23$ mm normalized by yield strength S_0 for two CT specimen sizes at approximately $J = 140$ N/mm.

approximated by a power law of (J/r) or (δ_t/r) which is of the same kind as the plane strain HRR solution. However, the quality of approximation differs strongly between the different tensor components.

(5) The HRR singularity field is not able to describe the stress state directly at the crack tip where large strains and crack tip blunting occurs. Hence, it can predict neither the values nor the loci of the maxima of the principal stresses ahead of the crack tip. But the plane strain HRR solutions adopted to the midplane of the CT specimen gave an upper bound of the tensile stresses in all other cases which is an important feature if it can be generalized.

(6) It is not yet clear how to quantify the approach to a plane strain situation in a 3D structure. The applicability of a plane strain HRR solution to a real structure is therefore still uncertain.

REFERENCES

1. J. W. Hutchinson, Fundamentals of the phenomonological theory of nonlinear fracture mechanics. *ASME J. Appl. Mech.* **50,** 1042–1051 (1983).
2. J. R. Rice, A path-independent integral and the approximate solution of strain concentration by notches and cracks. *ASME J. Appl. Mech.* **35,** 379–386 (1968).
3. J. W. Hutchinson, Singular behaviour at the end of a tensile crack in a hardening material. *J. Mech. Phys. Solids* **16,** 13–31 (1968).
4. J. R. Rice and G. F. Rosengren, Plane strain deformation near a crack tip in a power law hardening material. *J. Mech. Phys. Solids* **16,** 1–12 (1968).
5. R. M. McMeeking, Path dependence of the *J*-integral and the role of *J* as a parameter characterizing the near-tip field. *ASTM STP* **631,** 28–41 (1977).
6. A. Bakker, The three-dimensional *J*-integral—An investigation into its use for post-yield fracture safety assessment. Doctor Dissertation, Delft University of Technology, Delft (1984).
7. J. R. Rice and M. A. Johnson, The role of large crack tip geometry changes in plane strain fracture. In *Inelastic Behaviour of Solids* (Edited by M. F. Kanninen, W. F. Adler, A. R. Rosenfield and R. I. Jaffee), pp. 641–672. McGraw-Hill, New York (1970).
8. R. M. McMeeking, Finite deformation analysis of crack-tip opening in elastic–plastic materials and implication for fracture. *J. Mech. Phys. Solids* **25,** 357–381 (1977).
9. R. M. McMeeking and D. M. Parks, On criteria for *J*-dominance of crack tip fields in large-scale yielding. *ASTM STP* **668,** 175–194 (1979).
10. C. F. Shih, M. D. German and V. Kumar, An engineering approach for examining crack growth and stability in flawed structures. *J. Pres. Ves. Piping* **9,** 159–196 (1981).
11. G. Künecke, J. Olschewski and M. Zelewski, Three dimensional finite element analysis to predict the effect of size on elastic–plastic fracture parameters. 8th SMiRT, paper G 2/8 (1985).
12. D. Aurich, W. Brocks, H.-D. Noack and H. Veith, Fracture mechanics analysis of a pressure vessel with a semi-elliptical surface crack using elastic plastic finite element calculations. *ASTM 16th Nat. Symp. Fracture Mechanics*, Columbus (1983).
13. D. Aurich, W. Brocks, R. Jordan, J. Olschewski, H. Veith and J. Ziebs, The influence of multiaxial stress on characteristic parameters for cleavage fracture in the elastic–plastic range. *Proc. Int. Conf. Application of Fracture Mechanics to Materials and Structures*, pp. 345–355. Martinus Nijhoff, The Hague (1984).
14. ADINA—A Finite Element Program for Automatic Dynamic Incremental Nonlinear Analysis, Report AE 81, Watertown (1981).
15. J. Matzkows, R. Boddenberg and F. Kaiser, JINFEM—Postprozessor für das FEM-Programm ADINA zur Berechnung des *J*-Integrals, Berlin (1982).
16. D. M. Parks, Virtual crack extension—a general finite element technique for *J*-integral evaluation. *Proc. 1st Int. Conf. Numerical Methods in Fracture Mechanics*, pp. 464–478. Swansea (1978).
17. H. G. de Lorenzi, On the energy release rate and the *J*-integral for 3D crack configurations. *Int. J. Fracture* **19,** 183–193 (1982).